Stochastic Schrödinger equation for hot-carrier dynamics in plasmonic systems

Stochastic Schrödinger equation for hot-carrier dynamics in plasmonic systems

Giulia Dall'Osto,[1, a)] Mirko Vanzan,[2, 1] S. Corni,[1, 3] Margherita Marsili,[4, b)] and E. Coccia[5, c)]

[1)]*Dipartimento di Scienze Chimiche, Università di Padova, via F. Marzolo 1, 35131, Padova, Italy*

[2)]*Dipartimento di Fisica, Università di Milano, Via Giovanni Celoria 16, 20133, Milano, Italy*

[3)]*Istituto Nanoscienze-CNR, via Campi 213/A, 41125, Modena, Italy*

[4)]*Dipartimento di Fisica e Astronomia "Augusto Righi", University of Bologna, Viale Berti Pichat 6/2, 40127, Bologna, Italy*

[5)]*Dipartimento di Scienze Chimiche e Farmaceutiche, Università di Trieste, via L. Giorgieri 1, 34127, Trieste, Italy*

(Dated: 8 August 2024)

We present a multiscale method coupling the theory of open quantum systems with real-time ab initio treatment of electronic structure to study hot-carrier dynamics in photoexcited plasmonic systems. We combine the Markovian Stochastic Schrödinger equation (SSE) with an ab initio GW coupled to Bethe-Salpeter (BSE) equation description of the electronic degrees of freedom, interacting with a metallic nanoparticle modelled classically according to the polarizable continuum model. We apply this methodology to study the effect of relaxation (T_1) and pure dephasing (T_2) times on the hot-carrier dynamics in a system composed of a quantum portion described at GW/BSE level, i.e. a CHO fragment adsorbed on a vertex of a rhodium nanocube, and of the rest of the nanocube, treated classically, when irradiated with a 2.7 eV light pulse, inspired by the experimental results on plasmon-driven CO_2 photoreduction. A net hole injection from rhodium to CHO is observed, with and without the classical portion of the nanocube. The nanocube effect is to enhance the generated charge population by two orders of magnitude. The nonradiative decay, via a relaxation time T_1 based on the energy-gap law, produces a rapid decrease of the charge population. Results with T_2 only show that a charge injection retarded with respect to the pulse, which is present in the coherent dynamics, disappears when coherence is erased.

[a)]Electronic mail: giulia.dallosto@unipd.it
[b)]Electronic mail: margherita.marsili@unibo.it
[c)]Electronic mail: ecoccia@units.it

I. INTRODUCTION

Achieving fine control of light-matter interaction at the nanoscale could lead to great advances in many technological fields such as sensing, communication, medicine, catalysis and renewable energy.[1–5] In this sense, metallic nanoparticles (NPs) are particularly promising as they can efficiently absorb and confine electromagnetic radiation by activating the Localized Surface Plasmon Resonances (LSPRs).[6,7] As it decays, the energy stored in the LSPRs promotes the generation of electron-hole pairs which then separately thermalize, reaching a high-temperature equilibrium Fermi-Dirac distribution, as if the carriers (electron and holes) are heated up, in a typical time window of 1-100 fs.[2,8–17] Before they relax back to the lattice-temperature distribution through phonon scattering, these hot carriers (HCs) can be exploited to drive chemical reactions on the NP surface and this possibility provides a rationale for effective light-to-chemical energy conversion.[18–24] Despite the great interest this mechanism has collected in the past 15 years, its complexity has prevented the design of a complete and coherent framework for HCs mediated reactions to date. Such a phenomenon indeed involves multiple interacting species, namely the reacting molecules, NP, HCs and the external radiation. The dynamics and the interplay between those actors are intrinsically quantum, as the driven catalysis might be promoted by different quantum mechanisms such as HCs transfer, excited state dynamics, near-field enhanced intramolecular transitions, population of vibrational states, and carriers-phonon scattering.[25–32] In order to deal with such a complex picture, we developed a multiscale model that is able to properly treat the real-time dynamics of electrons in a molecular moiety absorbed on an optically excited NP,[33–37] encompassing continuum electrodynamics, Density Functional Theory (DFT) and post-DFT approaches such as GW coupled to Bethe-Salpeter Equation (BSE). Indeed, a multiscale modeling of the photoinduced electronic dynamics offers the possibility of including the entire NP, with its specific size and shape, sometimes enhancing and other times hindering phenomena happening within smaller scale simulations. However, most of the (few) multiscale studies of photoinduced electronic dynamics rely on real-time time-dependent DFT (TDDFT) either when coupling a jellium NP with an atomistic moiety[38,39] or when coupling a quantum moiety with a classical NP (either treated as a discrete collection of classical atoms or as a continuum)[40,41], and are, moreover, able to capture only the coherent evolution of the electronic system. Our methodology, instead, relies on a GW/BSE active space, overcoming TDDFT limitations concerning relative level alignments and the description of charge transfer excitations[42]. A real-time formulation of polarizable continuum

model (PCM) is then used to describe the polarization of a metal NP under the influence of an external electromagnetic pulse, in presence of a molecule or a cluster treated at quantum mechanical (QM) level of theory (DFT and GW/BSE here).[34,36,43–45] This time-dependent QM/continuum method is dubbed TD-PCM-NP.[36]

We recently applied this model to the study of rhodium-catalyzed CO_2 reduction.[45] Indeed, it was shown how Rh nanocubes selectively convert CO_2 into CH_4 when illuminated with an external radiation which frequency matches the LSPR on the nanocubes, in a hydrogen-rich environment.[46,47] We demonstrated that the efficiency of the photoexcited reaction resides in a NP-to-molecule hole injection that ease the pathway to CH_4 production by making the CHO fragment's oxygen more reactive. A deeper insight on the microscopic process guiding the injection, showed that the presence of the Rh nanocube promotes such a direct charge transfer due to the enhancement of near field intensity.[45]

Plasmon-mediated HC injection occurs in very short timescales concurrent with dephasing and nonradiative relaxation decays induced by rapid interaction with the surrounding environment.[48–51] In this framework, the system can no longer be considered close but rather open[52–55], meaning that dephasing and relaxation have to be properly accounted for a comprehensive understanding of the whole phenomena.[56–59] In the theory of open quantum systems, several approaches have been developed.[52,53,60–63] One method is the Lindblad[64,65] master equation for the reduced density matrix,[66–71] which provides a means to solve the problem under the Markovian limit[72–74] (i.e., when the environment relaxes at a faster rate than the system). Alternatively, another approach is rooted in the time evolution of the system wavefunction, known as the stochastic Schrödinger equation (SSE) in the Markovian limit.[63] SSE incorporates environmental interaction through stochastic and dissipative terms in each realization. As the number of trajectories tends to infinity, SSE yields results identical to those by the Lindblad equation[72,75] offering a computational advantage as it reduces the problem size by propagating the wavefunction instead of the density matrix. Among the variety of methods developed to practically solve SSE[76–79], the quantum jump algorithm, where the jumping probability is demanded to a Monte Carlo technique[43,80], has been widely used.[81,82]

SSE can be coupled to a quantum mechanical description of the system of interest[49,83,84], e.g. using TDDFT[78,85–87], Configuration Interaction Singles (CIS)[43,83], or GW/BSE equation.[44,45,63,88]

In this work, we use the TD-PCM-NP in combination with GW/BSE and SSE to study electron/hole dynamics[89–92] in the early steps of plasmon-mediated photoreduction of carbon dioxide

on rhodium nanocubes.[93] Specifically, we investigated the effect of pure dephasing and relaxation on the generation of electron and holes in the reaction intermediate CHO, when adsorbed on a rhodium corner, with and without the classical portion of the nanocube. The tool employed to analyze the HCs dynamics is the differential-projected density of states ΔPDOS[92] that provides the time evolution of the molecular orbitals population projected onto the atomic orbitals of a chosen fragment. Proper integration of ΔPDOS over energy provides the time evolution of charge population.

The present work is organized as follows: in Section II we show the theoretical model; computational details are collected in Section III; results are presented and discussed in Section IV, while conclusions are given in Section V.

II. THEORY

A. Stochastic Schrödinger equation

The time-evolution of the electronic wavefunction of the molecular target is modeled by the stochastic Schrödinger equation (SSE). This equation extends the traditional time-dependent Schrödinger equation to account for interactions with an external environment, allowing the treatment of the quantum system as open. SSE[34,43] has been implemented in the TDPlas-WaveT suite[94] within the Markovian limit[72] and it is given by:

$$i\frac{d}{dt}|\Psi_S(t)\rangle = \hat{H}(t)|\Psi_S(t)\rangle + \sum_q^M l_q(t)\hat{S}_q|\Psi_S(t)\rangle - \frac{i}{2}\sum_q^M \hat{S}_q^\dagger \hat{S}_q|\Psi_S(t)\rangle, \tag{1}$$

where the operator $\hat{S}_q$ is representative of the environment effect through the M interaction channels indexed by q. The dissipation induced by the environment is included by the non-Hermitian term $-\frac{i}{2}\sum_q^M \hat{S}_q^\dagger \hat{S}_q$. The fluctuation term $\sum_q^M l_q(t)\hat{S}_q$ is modeled by a Wiener process $l_q(t)$, also generated by the environment. The environment generates population and/or coherence relaxation, depending on the shape of $\hat{S}_q$. The system coincides with the electronic degrees of freedom of the QM portion, affected by the classical NP. Averaging the time-dependent coefficients on the number of independent SSE realizations, populations and coherences of the electronic states can be obtained.[43] The time dependent Hamiltonian $\hat{H}(t)$ includes the electronic field-free Hamiltonian $\hat{H}_0$ and the interaction with the incident pulse, when only the QM system is included:

$$\hat{H}(t) = \hat{H}_0 - \hat{\vec{\mu}} \cdot \vec{F}(t), \tag{2}$$

with $\vec{\hat{\mu}}$ the molecular dipole and $\vec{F(t)}$ the external pulse. The system wavefunction is expanded in the field-free eigenstates of $\hat{H}_0$

$$|\Psi_S(t)\rangle = \sum_{\lambda} C_\lambda(t)|\lambda\rangle. \tag{3}$$

We included two possible shapes for the operator $\hat{S}_q$ to account for pure dephasing and relaxation. The interaction channel q is here identified with the effect on a $|\lambda\rangle$ state, so we use the definition $\hat{S}_\lambda \equiv \hat{S}_q$.[43] The pure dephasing operator generates a coherence decay, keeping the population untouched. It is defined as[43]

$$\hat{S}_\lambda^{\text{dep}} = \sqrt{\gamma_\lambda/2}\sum_{\lambda'} P(\lambda',\lambda)|\lambda'\rangle\langle\lambda'|, \tag{4}$$

where $P(\lambda',\lambda)$ is equal to -1 if $\lambda' = \lambda$ or equal to 1 otherwise. Dephasing time T_2 is equal to the inverse of γ_λ, which is given as a phenomenological parameter. Since γ_λ is the same for any state pair, $T_2 = \frac{1}{\gamma}$. Even though energy-dependent T_2 values could in principle be considered, we have decided in the present work to use a single value of T_2, which means the same coherence decay for each pair of involved electronic states. This choice models an averaged environment effect on the coherence of the quantum system, and it somehow inspired by the works of Van Hulst and collaborators on the detection of electronic/vibronic coherence in single molecules[95,96]. A single value of T_2 can be considered as a limit case of a more realistic microscopic description, but accurate enough to capture the interaction between system and environment.

On the other hand, the relaxation accounts for population decay through nonradiative pathways. Here we propose a relaxation operator based on the well-known energy gap law[97–105], defined as

$$\hat{S}_\lambda^{\text{nonr}} = \sqrt{\Gamma_\lambda}|\lambda-1\rangle\langle\lambda| \tag{5}$$

with

$$\Gamma_\lambda = \alpha \exp\left[-\frac{\Delta E_\lambda}{\omega_v}\right], \tag{6}$$

where ΔE_λ ($\lambda > 0$) is the energy difference between $|\lambda\rangle$ and $|\lambda-1\rangle$ adjacent electronic states, ω_v is the vibrational frequency which mediates relaxation between adjacent states, and α is a constant. Subsequently, we will refer to $T_1 = \frac{1}{\alpha}$, which actually represents a lower limit to the T_1 resulting from Eq. 6. The energy gap law defines the rate of nonradiative decay between two electronic states of a molecular system as exponentially dependent on the energy gap ΔE_q.[98,99] The energy gap law is formulated within the assumptions that the electronic excitation is only weakly coupled to the vibrational structure of the molecule, and that the vibronic transition due to the highest frequency vibrational modes serves as the main route for the quantum transition mechanism.

B. TD-PCM-NP

The essentials of TD-PCM-NP are provided here. More details are available in Refs. 35,36,106. The NP is considered as a continuum system characterized by the polarization charges located in the center of its surface tesserae. The polarization charges follow the PCM equation in the integral equation formalism (IEF)[106–108] within the boundary element method (BEM). The time-dependent IEF-BEM charges enter the equation of the molecular electrodynamics as part of the Hamiltonian in presence of the polarizable NP, which now reads:

$$\hat{H}(t) = \hat{H}_0 - \hat{\vec{\mu}} \cdot \vec{F}(t) + (\mathbf{q}_{ref}(t) + \mathbf{q}_{pol}(t)) \cdot \hat{V}, \tag{7}$$

where $\mathbf{q}_{ref}(t)$ and $\mathbf{q}_{pol}(t)$ are the reflected and polarization charges generated respectively from the interaction with the incident pulse and with the molecular electrostatic potential $\hat{V}$.[33] Details on IEF-BEM charges are given in Supporting Information (SI).

In this multiscale case, Eq. 1 is propagated with the Hamiltonian of Eq. 7 and with the system wavefunction defined in the space of the eigenstates of a modified field-free Hamiltonian, accounting for the presence of the NP, as explained in Ref. 44. We couple here the GW-BSE QM description of the reactive part of the system to TD-PCM-NP.[44]

C. Analysis of the hot-carrier dynamics

When analyzing HC dynamics, a very useful tool is the ΔPDOS, introduced in Ref. 92 and applied in Ref. 45. The time-dependent $\Delta\text{PDOS}_K(t,\varepsilon)$ provides a two-dimensional map that displays the population of molecular orbitals, projected onto the atomic orbitals of a chosen fragment K, as a function of time t and energy ε. The subscript K refers to the fragment of the molecular system, defined in the simulations. As an example, in Ref. 92, the intramolecular charge transfer with dipole switching in LiCN has been studies, by defining Li and CN as fragments in ΔPDOS analysis. When integrated over the energy variable, $\Delta\text{PDOS}_K(t,\varepsilon)$ provides the time evolution of the overall electronic population or depopulation (hole population) of a given fragment, allowing to easily assess charge transfer or localization processes. For the single trajectory, i.e. a coherent

dynamics, the time dependent ΔPDOS is given by:

$$\begin{aligned}\Delta\text{PDOS}_K(t,\varepsilon) &= -\sum_i^{occ} w_i^K \text{Re}\left[\sum_{\lambda,\lambda'} C_\lambda^*(t)C_{\lambda'}(t)\sum_a^{vir} {d_{i,\lambda}^a}^* d_{i,\lambda'}^a\right] L_\eta(\varepsilon-\varepsilon_i) \\ &+ \sum_a^{vir} w_a^K \text{Re}\left[\sum_{\lambda,\lambda'} C_\lambda^*(t)C_{\lambda'}(t)\sum_i^{occ} {d_{i,\lambda}^a}^* d_{i,\lambda'}^a\right] L_\eta(\varepsilon-\varepsilon_a),\end{aligned} \tag{8}$$

where $C_\lambda(t)$ are the time-dependent coefficients of the expansion of the electronic wavefunction in terms of states $|\lambda\rangle$, that are eigenstates of H_0 (see Eq. 3) or of the modified field-free Hamiltonian with NP[44]. The $|\lambda\rangle$ states are linear combinations of singly excited Slater determinants in which an electron from the occupied state i is promoted to an empty states a, $d_{i,\lambda}^a$ being the coefficients of such expansion. $w_{i/a}^K$ are Lowdin weights. $L_\eta(\varepsilon-\varepsilon_i)$ are Lorentzian functions of center ε_i and width η.

Electron and hole populations generated in the fragment K of the QM system are given by:

$$\text{electron population} = \frac{1}{2}\int_{-\infty}^{\infty}[\Delta\text{PDOS}_K(t,\varepsilon)+|\Delta\text{PDOS}_K(t,\varepsilon)|]\,d\varepsilon \tag{9}$$

$$\text{hole population} = \frac{1}{2}\int_{-\infty}^{\infty}[\Delta\text{PDOS}_K(t,\varepsilon)-|\Delta\text{PDOS}_K(t,\varepsilon)|]\,d\varepsilon. \tag{10}$$

Eqs.9-10 consider any increase in the population of an orbital as electrons generated with respect to the ground state, and any decrease in such population as holes. These equations also apply to ground states with fractional orbital populations and reduce to the standard integration over empty or occupied energy ranges when orbitals are fully empty or fully occupied.

When analyzing an SSE dynamics the $\overline{C_\lambda^*(t)C_{\lambda'}(t)}$, i.e. the product of the $C_\lambda^*(t)$ coefficients averaged over all the trajectories are in principle needed, namely:

$$\begin{aligned}\Delta\text{PDOS}_K^{\text{SSE}}(t,\varepsilon) &= -\sum_i^{occ} w_i^K \text{Re}\left[\sum_{\lambda,\lambda'} \overline{C_\lambda^*(t)C_{\lambda'}(t)}\sum_a^{vir} {d_{i,\lambda}^a}^* d_{i,\lambda'}^a\right] L_\eta(\varepsilon-\varepsilon_i) \qquad (11)\\ &+ \sum_a^{vir} w_a^K \text{Re}\left[\sum_{\lambda,\lambda'} \overline{C_\lambda^*(t)C_{\lambda'}(t)}\sum_i^{occ} {d_{i,\lambda}^a}^* d_{i,\lambda'}^a\right] L_\eta(\varepsilon-\varepsilon_i). \qquad (12)\end{aligned}$$

Computational time can be saved by rewriting the average of the products between the time-dependent coefficients as $\overline{C_\lambda^*(t)C_{\lambda'}(t)} = \overline{C_\lambda^*(t)}\cdot\overline{C_{\lambda'}(t)} + \Delta_{\lambda\lambda'}(t)$, with $\Delta_{\lambda\lambda'}(t)$ being the covariance

of the products $C^*_\lambda(t)C_{\lambda'}(t)$. As shown in SI, ΔPDOS within SSE is thus given by

$$\begin{aligned}\Delta\mathrm{PDOS}_K^{\mathrm{SSE}}(t,\varepsilon) &= -\sum_i^{occ} w_i^K \mathrm{Re}\left[\sum_{\lambda,\lambda'} \overline{C^*_\lambda(t)}\cdot\overline{C_{\lambda'}(t)}\sum_a^{vir} {d^a_{i,\lambda}}^* d^a_{i,\lambda'}\right] L_\eta(\varepsilon-\varepsilon_i) \\ &+ \sum_a^{vir} w_a^K \mathrm{Re}\left[\sum_{\lambda,\lambda'} \overline{C^*_\lambda(t)}\cdot\overline{C_{\lambda'}(t)}\sum_i^{occ} {d^a_{i,\lambda}}^* d^a_{i,\lambda'}\right] L_\eta(\varepsilon-\varepsilon_i) + \mathscr{D}^k(t),\end{aligned} \tag{13}$$

where $\mathscr{D}^k(t) = -\sum_i^{occ} w_i^K \Delta_i(t) L_\eta(\varepsilon-\varepsilon_i) + \sum_a^{vir} w_a^K \Delta_a(t) L_\eta(\varepsilon-\varepsilon_a)$. $\Delta_i(t)$ and $\Delta_a(t)$ are defined in SI. Interestingly, because the terms $\Delta_{\lambda\lambda'}(t)$ represent the covariance of the products $C^*_\lambda(t)C_{\lambda'}(t)$, their contribution to the $\Delta\mathrm{PDOS}_K^{\mathrm{SSE}}(t,\varepsilon)$ given by $\mathscr{D}^k(t)$ might provide information on how much the trajectories are correlated.

Electron and hole population defined in Eqs. 9 and 10 are then extended to the SSE case by using $\Delta\mathrm{PDOS}_K^{\mathrm{SSE}}(t,\varepsilon)$ instead of $\Delta\mathrm{PDOS}_K(t,\varepsilon)$.

Details on the implementation are provided in SI.

III. COMPUTATIONAL DETAILS

We employed a multiscale approach to account for an extended Rh nanocube of 37 nm edge coupled with an atomistic cluster made by 19 Rh atoms positioned on the corner of the NP bonded to CHO residue.[45] CHO is the reaction intermediate of CH_4 formation, and it has been chosen because its dissociation into CH and O is the rate-determining step in the thermally activated reaction towards CH_4.[109,110] A representation of the simulate systems is reported in Figure 1 where the bare quantum (QM) system (panel a) or the whole QM/classical system (panel b) interacts with the pulse. The cut nanocube has been tessellated with 1143 tesserae of different dimensions, refining the region closer to the cut edge with smaller tesserae, and the edges curvature is equal to the radius of Rh atoms. One of the vertices of the nanocube is cut perpendicular to the (111) direction. Above the cut, we set the atomistic Rh_{19} cluster at the atomic interlayer distance, mimicking the vertex itself as shown in Figure 1b. The electronic energies and the transition dipole moments of the molecule are re-equilibrated with the polarization induced on the NP surface before performing the dynamics. The classical portion has been treated with TD-PCM-NP using the experimental dielectric function of rhodium.[111] The evolution algorithm assures that the total charge on the NP surface is neutral at each time step. The presence of the classical NP can modify the polarization of the quantum system and can provide for electromagnetic enhancement of the quantum system

response, but chemical interaction or charge transfer between classical and quantum system are not included. We tested the effect of an intermediate empty region between the NP and the quantum system as reported in the SI of Ref. 45.

The preparation of the computational system including geometry optimization and excited state calculations has been described in Ref. 45. For the sake of the reader, we repeat here the details. The atomistic structure of Rh_{19} has been extracted from a Rh(111) slab optimized at DFT level with Quantum Espresso, version 6.3.[112,113] We used a plane waves basis set and PBE functional while the core-electrons were modelled with the Optimized Norm-Conserving Vanderbilt pseudopotential[114] and the energy cut-off for the basis set expansion was set to 1080 eV. The system's geometry was optimized using a 8x8x1 k-point grid, with an additional 20 Å vacuum layer added perpendicular to the surface direction to prevent the formation of spurious electric fields.[115] While keeping the two bottom layers fixed in their ideal bulk positions, all other atoms were relaxed utilizing the Broyden–Fletcher–Goldfarb–Shanno quasi-Newton algorithm[116] until the residual forces fell below 10^{-4} eV/Å. Convergence was achieved with a threshold of 10^{-9} eV for the ground state total energy. Rh_{19} was extracted from the two outermost layers of the slab and employed as a substrate for the geometry optimization of CHO species performed with DFT at PBE/DZ level of theory by means of AMS code.[117] The DFT ground state, and 454 electronic excited states computed at BSE level of theory[44,45] have been employed in the electron dynamics calculation for expansion in Eq. 3. We have considered 435 occupied and 393 virtual molecular orbitals. DFT and BSE calculations have been carried out at PBE0/def2-TZVP level. Details about BSE within TD-PCM-NP are found in Refs. 45 and 44.

Electron dynamics, with and without the classical NP, have been carried out with the WaveT/TDPlas code.[36,106] We have employed a Gaussian envelope function for the time-dependent external field:

$$\vec{\mathrm{F}}(t) = \vec{\mathrm{F}}_{\max} \exp\left[-\frac{(t-t_0)^2}{2\sigma^2}\right] \sin(\omega t), \tag{14}$$

where $\vec{\mathrm{F}}_{\max}$ is the field amplitude (the intensity I_{max} is equal to $\frac{1}{2}|\vec{\mathrm{F}}_{\max}|^2$), t_0 and σ are the center and the amplitude of the Gaussian respectively, and ω is the pulse frequency. We employed a 459 nm as pulse wavelength, with FWHM equal to 23 fs and intensity $I_{max} = 3.3 \times 10^4$ W/cm^2, linearly polarized perpendicular to the vertex of the nanocube. A second-order Euler algorithm[33] was used to propagate Eq. 1. We simulated 100 fs with a time step of 1.21 as. 768 SSE trajectories

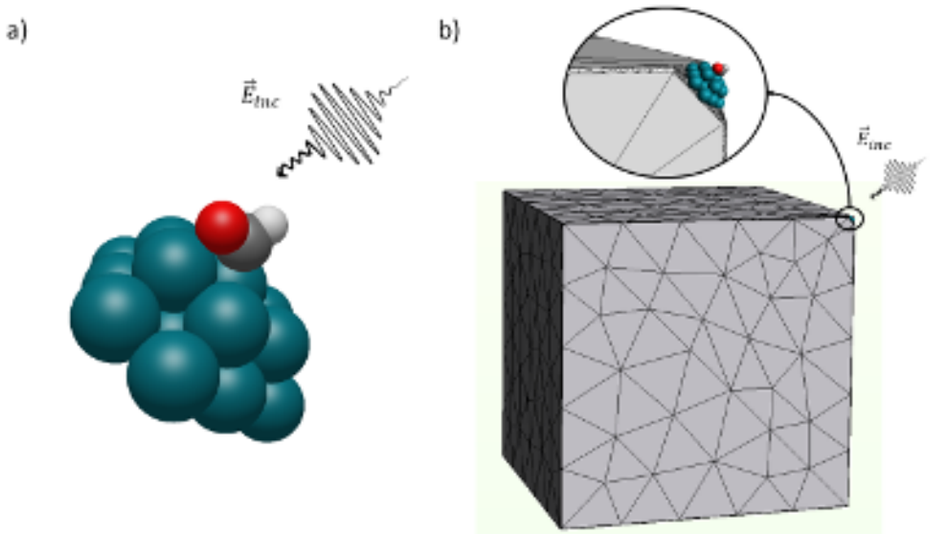

FIG. 1: a) Representation of the QM system Rh_{19}-CHO interacting with the incident electric field. b) Representation of the QM system coupled with the Rh nanocube.

have been carried out for each condition of dephasing and relaxation considered. In order to assess convergence with respect to the number of trajectories employed, we performed calculations also with 100, 300 and 600 trajectories for a chosen case with both pure dephasing and relaxation (T_2 = 5 fs and T_1 = 100 fs), verifying that charge population dynamics is fully converged with 768 trajectories. The results are reported in Figure 1 of SI. MPI parallel protocol has been used, with one SSE trajectory per MPI process. Performance of our MPI implementation is reported in the SI as weak and strong scaling (Figures 2 and 3) on a model system composed of LiCN (500 excited states) as QM system and a spherical gold NP (370 tesserae).

A homemade Fortran90 code has been used to compute the ΔPDOS and its integral in order to compute electron and hole populations. The amplitude of the Lorentzian function is 0.0272 eV and the energy grid used to compute ΔPDOS and its integration goes from -21.7 eV to 21.7 eV with a step of 0.0217 eV. The post-processing calculation has been performed considering two fragments (CHO and all rhodium atoms).

IV. RESULTS AND DISCUSSION

This section presents the key findings derived from our simulations, aimed to show the effects

of the relaxation and pure dephasing on the charge population in the systems reported in Figure 1. After performing the electronic dynamics of the QM system (in absence of the continuum NP, Figure 1a), the wavefunction coefficients were used to compute the ΔPDOS and the electron and hole populations in the whole system.

In this case, the total ΔPDOS, i.e. using the original nonprojected density of states (no fragment is defined), has been used in Eqs. 9-10.

Analyzing the results of coherent dynamics with a different pulse frequency in a recent work[45], we explained the experimental selectivity towards methane against carbon monoxide in the photocatalytic reaction of carbon dioxide hydrogenation on rhodium with the net hole injection into the CHO fragment, which makes the oxygen atom the most reactive species. Details are found in Ref. 45. We anticipate that this interpretation still holds true in the presence of T_1 and T_2.

Figure 2 illustrates the temporal evolution of absolute hole and electron populations under var-

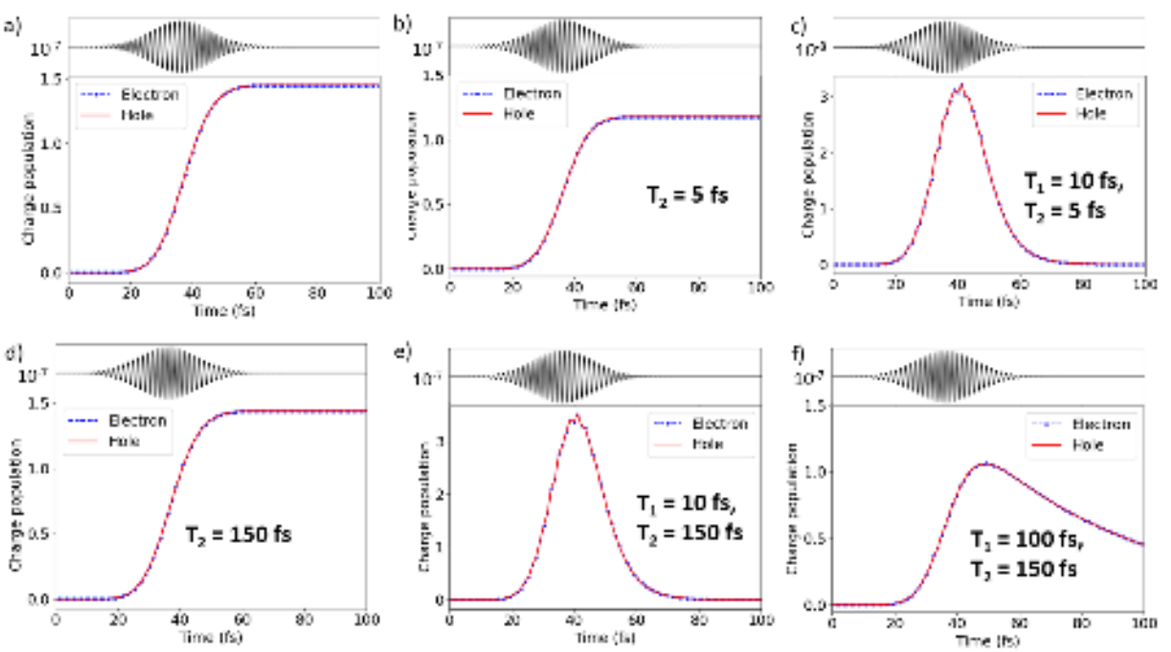

FIG. 2: Time-evolution of the photoinduced charge carrier populations (electron and hole) in the quantum part (Rh_{19} - CHO) in presence of different dephasing and relaxation conditions: a) without relaxation or dephasing, b) in presence of dephasing only with T_2 = 5 fs, c) including dephasing with T_2 = 5 fs and relaxation with T_1 = 10 fs, d) in presence of only dephasing with T_2 = 150 fs, e) including dephasing with T_2 = 150 fs and relaxation with T_1 = 10 fs and f) including dephasing with T_2 = 150 fs and relaxation with T_1 = 100 fs.

ious dephasing and relaxation conditions. The maximum charge population is generated when dephasing or relaxation events are absent (panel a), i.e. for a coherent dynamics. A similar result is obtained in presence of slow dephasing decay, such as in panel d) with T_2 = 150 fs when the dephasing process has a longer timescale than the electric field duration. The charge population has a flat profile when no relaxation decay is included, which highlights that populations weight more than coherences in the calculation of time changes of ΔPDOS, as in Eq. 11. The effect of coherence decay, induced by pure dephasing, is indicated by a decreasing on the maximum charge population generated, which is much more evident with fast dephasing time (panel b). On the other hand, when both dephasing and relaxation channels are incorporated into the model, as shown in panels c), e) and f), the charge population decreases over time, with a decay rate determined by the relaxation time T_1. Moreover, the charge population generated decreases when fast relaxation is considered. It becomes evident that when relaxation processes occur within the timescale of HC generation, i.e. $\sim 1 - 100$ fs[2,13,14,16,17], is essential to include them in the modeling to achieve an accurate simulation of a realistic system.

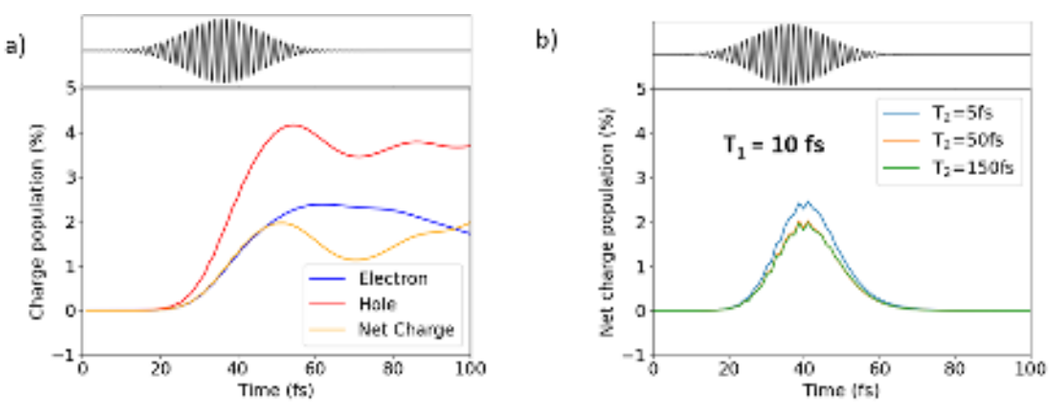

FIG. 3: a) Time-evolution of the photoinduced charge carrier population into CHO (%) in absence of dephasing or relaxation. b) Time-evolution of the photoinduced net charge population into CHO (%) in presence of relaxation with T_1 = 10 fs and different values of dephasing: T_2 = 5 fs, T_2 = 50 fs,T_2 = 150 fs.

Furthermore, the relative electron and hole population were computed, dividing the QM portion into two fragments: the reaction intermediate CHO and the rhodium atoms. In Figure 3a) the charge population percentage on CHO fragment has been reported as a function of time for

different simulation conditions. The charge population percentage is obtained, dividing the electron (hole) population by the maximum electron (hole) population generated in the whole system (Rh_{19}-CHO) during the dynamics. The net charge, computed as the difference between hole and electron charges, is also shown. In any case, the hole injection mechanism on the CHO fragment prevails, as already highlighted in ref. 45. The charge population percentage reported in panel a) is computed in the absence of dephasing or relaxation, resulting in a steady charge population without an overall decrease. The hole population shows two maxima: one right after the interaction with the incident peaks and another after 80 fs, suggesting a two-step hole injection mechanism.[45] The electron dynamics is smoother in general because the carriers injected during the dynamics are holes rather than electrons. It is also highlighted in Figure 4 of SI, which shows hole depletion on Rh_{19} fragment with the same profile, but opposite phase, as for CHO fragment.

The effect of a relaxation time T_1 = 10 fs combined with different dephasing times is shown in Figure 3b in terms of net charge population percentage. Hole and electron dynamics have been reported in Figure 5 of SI. The rapid relaxation mechanism manifests as a charge population decay right after the end of the interaction with the incident pulse and small peaks in correspondence to the maximum, attributed to the swift depopulation and repopulation of states. The only observable difference in Figure 3b induced by varying the dephasing time appears on the net charge population percentage, which is slightly higher with faster dephasing time while for slower dephasing processes the two lines are superimposed.

We have analysed the time evolution of charge population percentages with dephasing times T_2 = 5 fs in Figure 4 and T_2 = 150 fs in Figure 5 and varying relaxation time. Data are also collected in Figures 6 and 7 of SI. Including a fast dephasing time, charge population oscillations visible in the coherent dynamics are not present, thus the second hole injection mechanism, not induced by the electric field, is produced by long-lived coherences. This is important as it shows that an indirect (or better: retarded) charge-injection may exist still based on the coherent evolution of the wave function, different from the incoherent indirect charge injection mechanism that is usually considered. Moreover, electron population percentage generated is even lower than in absence of dephasing. Preference of hole generation on CHO, rather than electron generation, is slightly improved with fast decoherence mechanism, although including a decoherence mechanism is not crucial for the realization of the process. The impact of including and varying the relaxation time is manifested as charge population decay after the interaction with the incident field with the rate of relaxation process, as shown by Figure 4b.

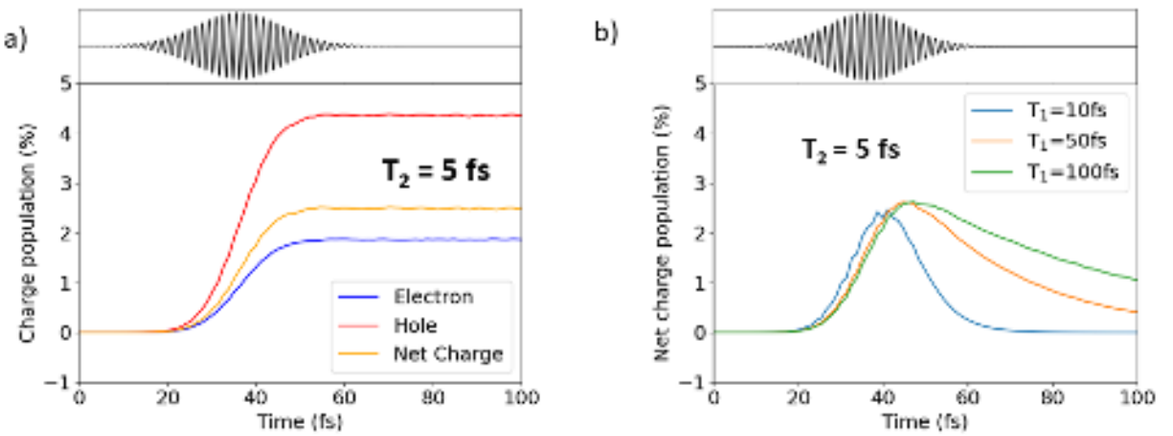

FIG. 4: a) Time-evolution of the photoinduced charge carrier population into CHO (%) in presence of dephasing with T_2 = 5 fs without including relaxation. b) Time-evolution of the photoinduced net charge population into CHO (%) in presence of dephasing with T_2 = 5 fs and different values of relaxation: T_1 = 10 fs, T_1 = 50 fs, T_1 = 100 fs.

On the other hand, when slower dephasing time is included (T_2 = 150 fs, panel a) of Figure 5) the charge population percentage dynamics approaches the coherent case (Figure 3a) in which the hole population percentage achieves two maxima. The results of calculations performed with different relaxation times in Figure 5b show a decay profile of the net charge population determined by the T_1 employed. They are very similar to Figure 4b obtained with faster dephasing time, but for the maximum charge population percentage, which is slightly lower in this case. Only with the slowest relaxation time T_1 = 100 fs oscillations of net charge population are slightly visible as effect of the long-lived coherences.

We have studied the possible effect of the size of the rhodium corner on the hot-carrier dynamics, by comparing rhodium clusters with 19 atoms (2 layers, the system presented here) and with 37 atoms (3 layers): we expect the predicted photocatalysis mechanism (hole injection into CHO) to remain the same with increasing size of the quantum portion, as detailed in SI (Figures 8-10 and corresponding discussion).

Finally, simulations have also been performed, including the classically described NP as a continuum (Figure 1b). In Figure 6, we report two cases in which both decay processes have been

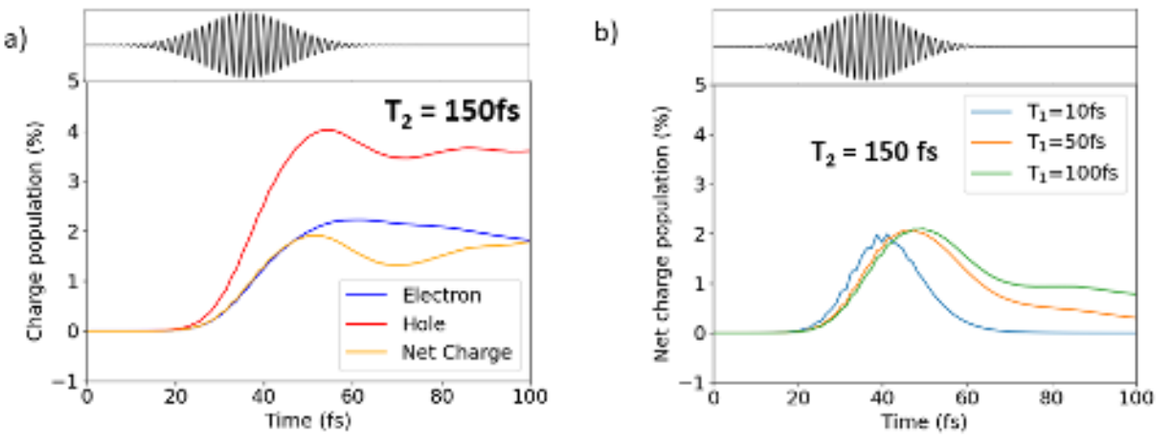

FIG. 5: Time-evolution of the photoinduced charge carrier population into CHO (%) in presence of dephasing with T_2 = 150 fs without including relaxation (a) and including different values of relaxation : b) T_1 = 10 fs, c) T_1 = 50 fs, d) T_1 = 100 fs.

included in the description. A noteworthy observation is that when the classical NP is included, the overall charge population generated is at least two orders of magnitude higher compared to calculations carried out without it (shown in Figure 2). Similarly to the scenario without the classical NP, the presence of the smaller relaxation time T_1 = 50 fs (panel a) results in a lower charge population that decays more rapidly compared to the case with T_1 = 100 fs (panel b).

Results with the full system of Figure 1b agree well with literature estimations of HC generation rate and incident photon conversion efficiency.[45]

V. CONCLUSIONS

We present here a real-time multiscale approach to study the HC dynamics in complex systems using SSE for describing environmental effects. Taking inspiration from the experimental photoreduction of carbon dioxide on rhodium nanocubes[46], we defined a QM model composed of two rhodium layers mimicking the nanocube corner, and the CHO reaction intermediate adsorbed on it. The full system, also including the classical part of the nanocube, is described using the TD-PCM-NP approach. Our real-time (multiscale) approach provided electron and hole population on CHO and rhodium layers. The effect of the pure dephasing is to lower the maximum value of the charge population and to suppress indirect hole injection, in the simulations where the latter were present.

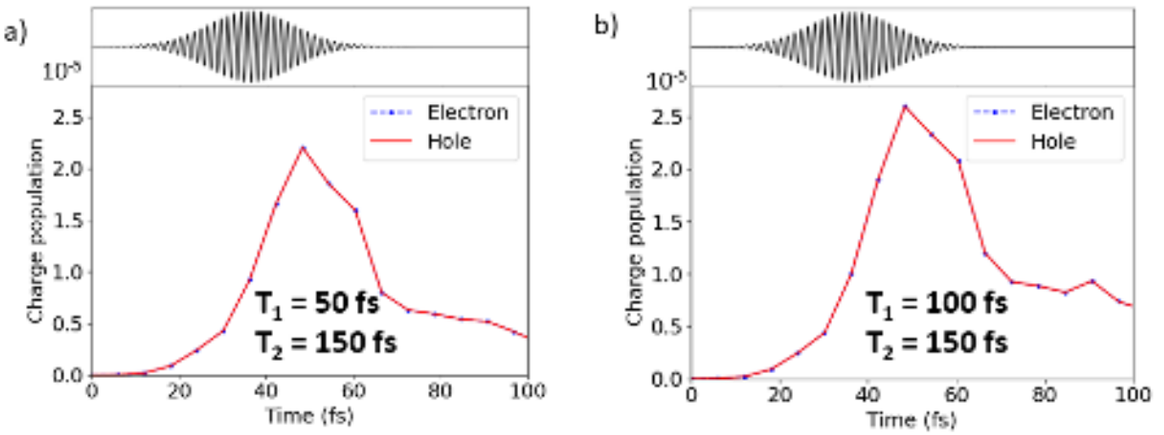

FIG. 6: Time-evolution of the photoinduced charge carrier population into CHO-Rh_{19} system in multiscale calculation when the quantum system is coupled with the classical rhodium nanocube, in presence of dephasing with T_2 = 150 fs and relaxation with T_1 = 50 fs (a), including dephasing with T_2 = 150 fs and relaxation with T_1 = 100 fs (b). Electron and hole populations are superimposed as the system is neutral.

Such a result points to the possibility of an indirect, but still coherent, charge injection that is different from what has been identified so far; it is probably better to use the term retarded coherent charge injection for this new mechanism. Simulating a nonradiative decay, via a relaxation time T_1 defined within the energy-gap law, produces a rapid decrease of the charge population. Including the continuum NP in the description determines the enhancement of charge population generated by two order of magnitude, as obtained also in previous calculations.[45] The approach developed allowed to include relaxation and dephasing decay mechanisms that profoundly affects the charge population dynamics, in order to fill the gap with a realistic fast HC dynamics occurring under the influence of external and plasmonic fields.

We are aware that the use of density matrix-based methods for systems such as ours (455 electronic states) may prove more efficient than an SSE-based approach. However, using SSE is advantageous in multiscale approaches with a quantum description of the system for two reasons: 1) coupling SSE to quantum chemistry codes is natural and conceptually simple, since the main object is the wavefunction; 2) SSE is embarrassing parallel, as we show in SI, so we can harness the power of supercomputers.

ACKNOWLEDGMENTS

Financial support from ICSC – Centro Nazionale di Ricerca in High Performance Computing, Big Data and Quantum Computing, funded by European Union – NextGenerationEU is gratefully acknowledged. This work has been supported by the project CHANGE funded by the PRIN 2022 - Progetti di Rilevante Interesse Nazionale (grant 20224KAC28). M.V. is grateful to the COSY Action CA21101 financed by the European Cooperation in Science and Technology (COST) programme. M.V. also acknowledges University of Milan for funding his postdoctoral fellowships "La bellezza degli aggregati: da nano a astro particelle". EC thanks Mauro Stener and Daniele Toffoli for helpful discussions.

SUPPORTING INFORMATION

Theory details on TD-PCM-NP and on an efficient implementation of the ΔPDOS; convergence study with respect to the number of trajectories; Weak and strong scaling for SSE parallel calculations; data on charge-population dynamics; analysis of size effects of the rhodium corner.

DATA AVAILABILITY

The data that support the findings of this study are available from the corresponding author upon reasonable request.

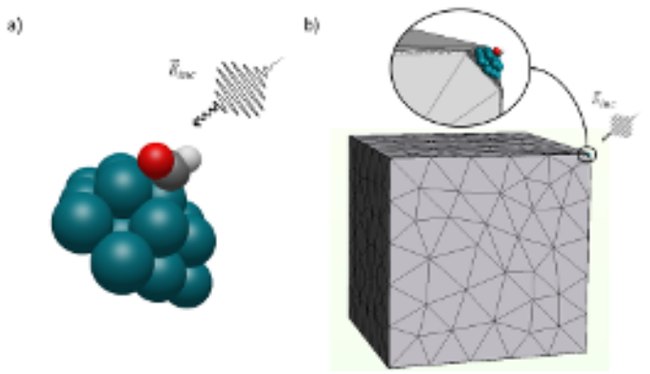

Figure 1: a) Representation of the QM system Rh_{19}-CHO interacting with the incident electric field. b) Representation of the QM system coupled with the Rh nanocube.

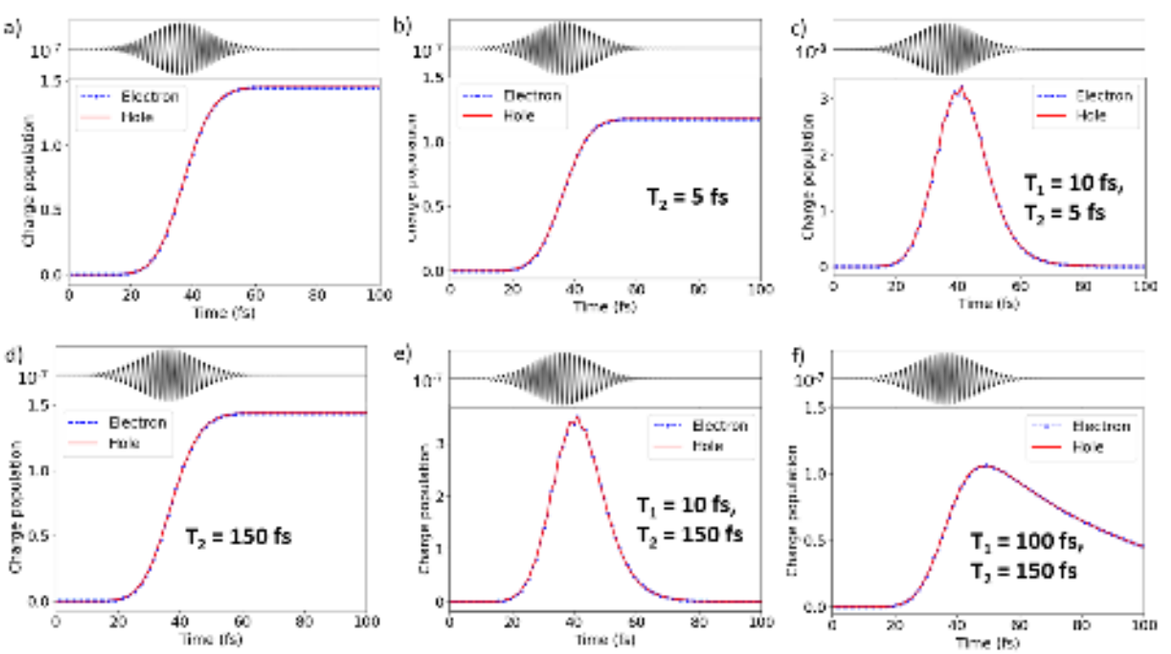

Figure 2: Time-evolution of the photoinduced charge carrier populations (electron and hole) in the quantum part (Rh_{19} - CHO) in presence of different dephasing and relaxation conditions: a) without relaxation or dephasing, b) in presence of dephasing only with T_2 = 5 fs, c) including dephasing with T_2 = 5 fs and relaxation with T_1 = 10 fs, d) in presence of only dephasing with T_2 = 150 fs, e) including dephasing with T_2 = 150 fs and relaxation with T_1 = 10 fs and f) including dephasing with T_2 = 150 fs and relaxation with T_1 = 100 fs.

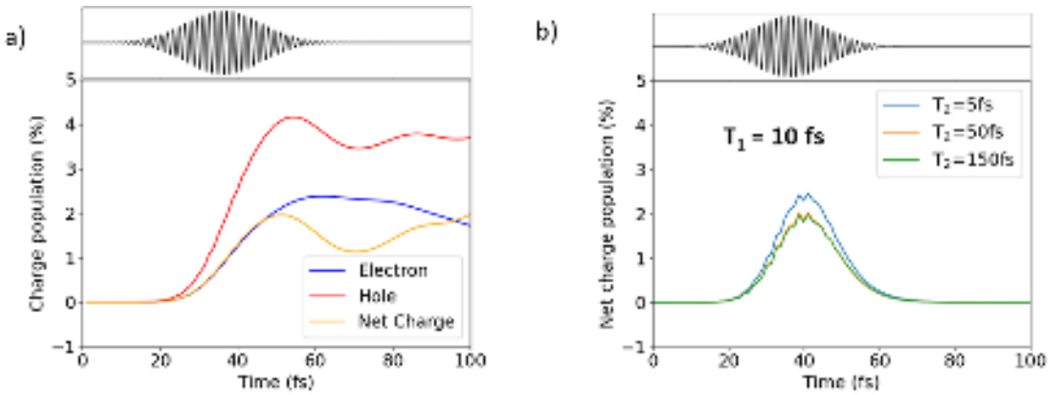

Figure 3: a) Time-evolution of the photoinduced charge carrier population into CHO (%) in absence of dephasing or relaxation. b) Time-evolution of the photoinduced net charge population into CHO (%) in presence of relaxation with T_1 = 10 fs and different values of dephasing: T_2 = 5 fs, T_2 = 50 fs,T_2 = 150 fs.

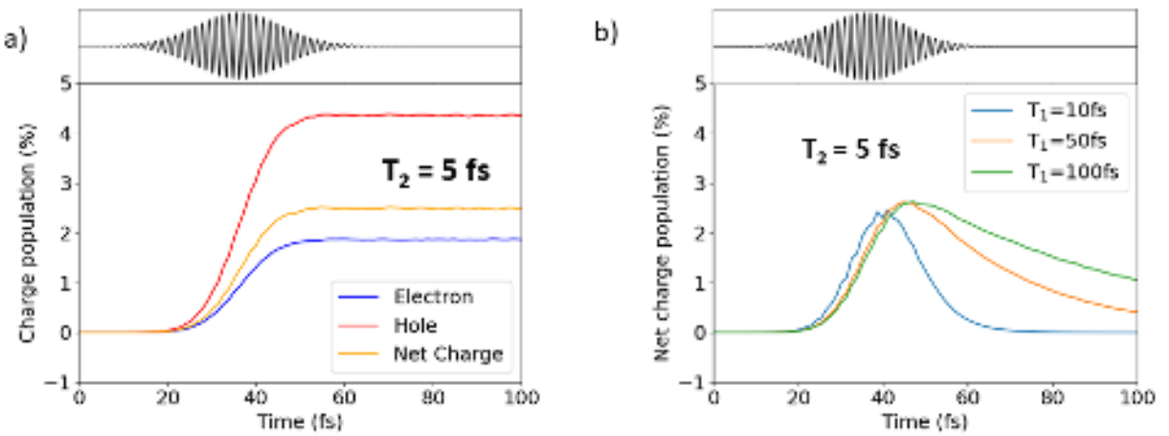

Figure 4: a) Time-evolution of the photoinduced charge carrier population into CHO (%) in presence of dephasing with T_2 = 5 fs without including relaxation. b) Time-evolution of the photoinduced net charge population into CHO (%) in presence of dephasing with T_2 = 5 fs and different values of relaxation: T_1 = 10 fs, T_1 = 50 fs, T_1 = 100 fs.

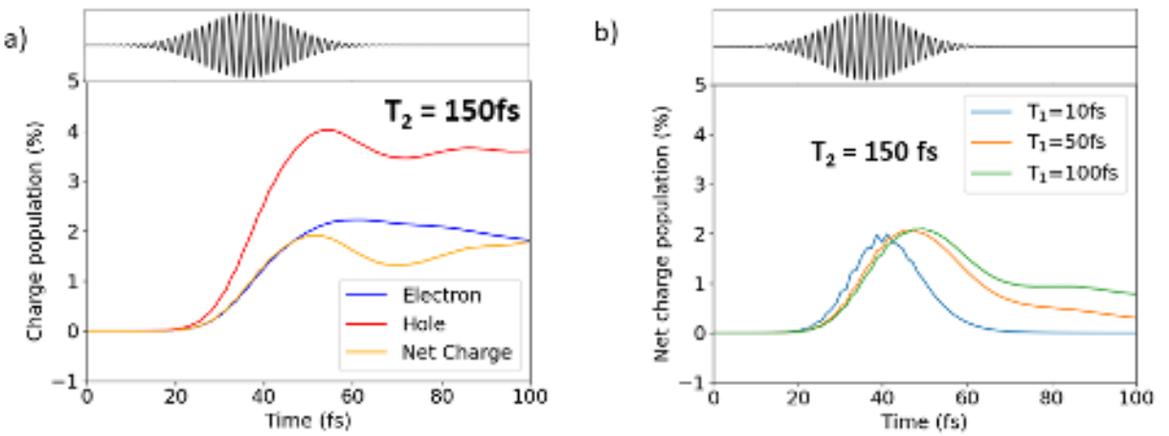

Figure 5: Time-evolution of the photoinduced charge carrier population into CHO (%) in presence of dephasing with T_2 = 150 fs without including relaxation (a) and including different values of relaxation : b) T_1 = 10 fs, c) T_1 = 50 fs, d) T_1 = 100 fs.

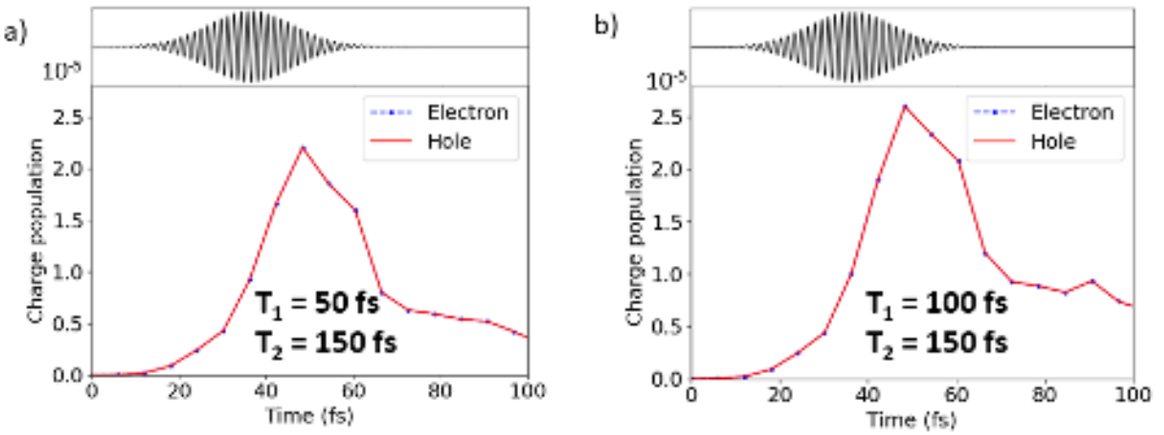

Figure 6: Time-evolution of the photoinduced charge carrier population into CHO-Rh_{19} system in multiscale calculation when the quantum system is coupled with the classical rhodium nanocube, in presence of dephasing with T_2 = 150 fs and relaxation with T_1 = 50 fs (a), including dephasing with T_2 = 150 fs and relaxation with T_1 = 100 fs (b). Electron and hole populations are superimposed as the system is neutral.

REFERENCES

[1]U. Aslam, V. G. Rao, S. Chavez, and S. Linic, "Catalytic conversion of solar to chemical energy on plasmonic metal nanostructures," Nat. Catal. **1**, 656–665 (2018).

[2]M. L. Brongersma, N. J. Halas, and P. Nordlander, "Plasmon-induced hot carrier science and technology," Nat. Nanotech. **10**, 25–34 (2015).

[3]A. B. Zrimsek, N. Chiang, M. Mattei, S. Zaleski, M. O. McAnally, C. T. Chapman, A. I. Henry, G. C. Schatz, and R. P. V. Duyne, "Single-Molecule Chemistry with Surface- and Tip-Enhanced Raman Spectroscopy," Chem. Rev. **117**, 7583 (2017).

[4]A. Longato, M. Vanzan, E. Colusso, S. Corni, and A. Martucci, "Enhancing Tungsten Oxide Gasochromism with Noble Metal Nanoparticles: The Importance of the Interface," Small **19**, 2205522–11 (2023).

[5]N. Jiang, X. Zhuo, and J. Wang, "Active Plasmonics: Principles, Structures, and Applications," Chem. Rev. **118**, 3054–3099 (2018).

[6]S. A. Maier, *Plasmonics: Fundamentals and Applications* (Springer, 2007).

[7]A. N. Koya, M. Romanelli, J. Kuttruff, N. Henriksson, A. Stefancu, G. Grinblat, A. De Andres, F. Schnur, M. Vanzan, M. Marsili, M. Rahaman, A. V. Rodríguez, T. Tapani, H. Lin, B. D. Dana, J. Lin, G. Barbillon, R. P. Zaccaria, D. Brida, D. Jariwala, L. Veisz, E. Cortes, S. Corni, D. Garoli, and N. Maccaferri, "Advances in ultrafast plasmonics," Appl. Phys. Rev. **10**, 021318–38 (2023).

[8]R. Sundararaman, P. Narang, A. S. Jermyn, W. A. Goddard, and H. A. Atwater, "Theoretical predictions for hot-carrier generation from surface plasmon decay," Nat. Commun. **5**, 5788 (2014).

[9]P. Christopher and M. Moskovits, "Hot Charge Carrier Transmission from Plasmonic Nanostructures," Annu. Rev. Phys. Chem. **68**, 379–398 (2017).

[10]P. Narang, R. Sundararaman, and H. A. Atwater, "Plasmonic hot carrier dynamics in solid-state and chemical systems for energy conversion," Nanophotonics **5**, 96–111 (2016).

[11]A. Manjavacas, J. G. Liu, V. Kulkarni, and P. Nordlander, "Plasmon-induced hot carriers in metallic nanoparticles," ACS Nano **8**, 7630–7638 (2014).

[12]Z. Zhang, L. Liu, W.-H. Fang, R. Long, M. V. Tokina, and O. V. Prezhdo, "Plasmon-mediated electron injection from Au nanorods into MoS_2: traditional versus photoexcitation mechanism," Chem **4**, 1112–1127 (2018).

[13]E. Kazuma and Y. Kim, "Mechanistic Studies of Plasmon Chemistry on Metal Catalysts," Angew. Chem. Int. Ed. **58**, 4800–4808 (2019).

[14]Z. Li and D. Kurouski, "Plasmon-Driven Chemistry on Mono- And Bimetallic Nanostructures," Accounts of Chemical Research **54**, 2477–2487 (2021).

[15]A. M. Brown, R. Sundararaman, P. Narang, W. A. Goddard, and H. A. Atwater, "Nonradiative plasmon decay and hot carrier dynamics: Effects of phonons, surfaces, and geometry," ACS Nano **10**, 957–966 (2016).

[16]A. M. Brown, R. Sundararaman, P. Narang, A. M. Schwartzberg, W. A. Goddard, and H. A. Atwater, "Experimental and ab initio ultrafast carrier dynamics in plasmonic nanoparticles," Phys. Rev. Lett. **118**, 087401 (2017).

[17]X. Li, D. Xiao, and Z. Zhang, "Landau damping of quantum plasmons in metal nanostructures," New Journal of Physics **15**, 023011 (2013).

[18]D. F. Swearer, H. Zhao, L. Zhou, C. Zhang, H. Robatjazi, J. M. P. Martirez, C. M. Krauter, S. Yazdi, M. J. McClain, E. Ringe, E. A. Carter, P. Nordlander, and N. J. Halas, "Heterometallic antenna-reactor complexes for photocatalysis," Proc. Natl. Acad. Sci. U.S.A. **113**, 8916–8920

(2016).

[19]C. Zhang, H. Zhao, L. Zhou, A. E. Schlather, L. Dong, M. J. McClain, D. F. Swearer, P. Nordlander, and N. J. Halas, "Al-Pd Nanodisk Heterodimers as Antenna–Reactor Photocatalysts," Nano Lett. **16**, 6677–6682 (2016).

[20]D. F. Swearer, R. K. Leary, R. Newell, S. Yazdi, H. Robatjazi, Y. Zhang, D. Renard, P. Nordlander, P. A. Midgley, N. J. Halas, and E. Ringe, "Transition-Metal Decorated Aluminum Nanocrystals," ACS Nano **11**, 10281–10288 (2017).

[21]D. F. Swearer, H. Robatjazi, J. M. P. Martirez, M. Zhang, L. Zhou, E. A. Carter, P. Nordlander, and N. J. Halas, "Plasmonic Photocatalysis of Nitrous Oxide into N_2 and O_2 Using Aluminum–Iridium Antenna–Reactor Nanoparticles," ACS Nano **13**, 8076–8086 (2019).

[22]Z. Zhang, C. Zhang, H. Zheng, and H. Xu, "Plasmon-Driven Catalysis on Molecules and Nanomaterials," Acc. Chem. Res. **52**, 2506–2515 (2019).

[23]L. Zhou, J. M. P. Martirez, J. Finzel, C. Zhang, D. F. Swearer, S. Tian, H. Robatjazi, M. Lou, L. Dong, L. Henderson, P. Christopher, E. A. Carter, P. Nordlander, and N. J. Halas, "Light-driven methane dry reforming with single atomic site antenna-reactor plasmonic photocatalysts," Nature Energy **5**, 61–70 (2020).

[24]L. Zhou, M. Lou, J. L. Bao, C. Zhang, J. G. Liu, J. M. P. Martirez, S. Tian, L. Yuan, D. F. Swearer, H. Robatjazi, E. A. Carter, P. Nordlander, and N. J. Halas, "Hot carrier multiplication in plasmonic photocatalysis," PNAS **118**, e2022109118 (2021).

[25]E. Cortés, L. V. Besteiro, A. Alabastri, A. Baldi, G. Tagliabue, A. Demetriadou, and P. Narang, "Challenges in Plasmonic Catalysis," ACS Nano **14**, 16202–16219 (2020).

[26]J. M. P. Martirez and E. A. Carter, "Prediction of a low-temperature N_2 dissociation catalyst exploiting near-IR-to-visible light nanoplasmonics," Sci. Adv. **3**, eaao4710 (2017).

[27]L. Zhou, D. F. Swearer, C. Zhang, H. Robatjazi, H. Zhao, L. Henderson, L. Dong, P. Christopher, E. A. Carter, P. Nordlander, and N. J. Halas, "Quantifying hot carrier and thermal contributions in plasmonic photocatalysis," Science **362**, 69–72 (2018).

[28]S. Linic, S. Chavez, and R. Elias, "Flow and extraction of energy and charge carriers in hybrid plasmonic nanostructures," Nat. Mater. **15**, 916–924 (2021).

[29]Y. Sivan and Y. Dubi, "Recent developments in plasmon-assisted photocatalysis - A personal Perspective," Appl. Phys. Lett. **117**, 130501 (2020).

[30]P. K. Jain, "Taking the Heat Off of Plasmonic Chemistry," J. Phys. Chem. C **123**, 24347–24351 (2019).

[31]M. Vanzan, T. Cesca, B. Kalinic, C. Maurizio, G. Mattei, and S. Corni, "Lanthanide ions sensitization by small noble metal nanoclusters," ACS Photonics **8**, 1364–1376 (2021).

[32]M. Vanzan, G. Gil, D. Castaldo, P. Nordlander, and S. Corni, "Energy Transfer to Molecular Adsorbates by Transient Hot Electron Spillover," Nano Lett. **23**, 2719–2725 (2023).

[33]S. Pipolo and S. Corni, "Real-time description of the electronic dynamics for a molecule close to a plasmonic nanoparticle," J. Phys. Chem. C **120**, 28774–28781 (2016).

[34]E. Coccia and S. Corni, "Role of coherence in the plasmonic control of molecular absorption," J. Chem. Phys. **151**, 044703 (2019).

[35]G. Dall'Osto, G. Gil, S. Pipolo, and S. Corni, "Real-time dynamics of plasmonic resonances in nanoparticles described by a boundary element method with generic dielectric function," J. Chem. Phys. **153**, 184114 (2020).

[36]E. Coccia, J. Fregoni, C. A. Guido, M. Marsili, S. Pipolo, and S. Corni, "Hybrid theoretical models for molecular nanoplasmonics," J. Chem. Phys. **153** (2020).

[37]M. Capone, M. Romanelli, D. Castaldo, G. Parolin, A. Bello, G. Gil, and M. Vanzan, "A vision for the future of multiscale modeling," ACS Phys. Chem. Au **4**, 202 (2024).

[38]C. Zhan, X. J. Chen, J. Yi, J. F. Li, D. Y. Wu, and Z. Q. Tian, "From plasmon-enhanced molecular spectroscopy to plasmon-mediated chemical reactions," Nat. Rev. Chem. **2**, 216–230 (2018).

[39]L. Yan, F. Wang, and S. Meng, "Quantum mode selectivity of plasmon-induced water splitting on gold nanoparticles," ACS Nano **10**, 5452–5458 (2016), https://doi.org/10.1021/acsnano.6b01840.

[40]J. Huang, X. Zhao, X. Huang, and W. Liang, "Understanding the mechanism of plasmon-driven water splitting: Hot electron injection and a near field enhancement effect," Physical Chemistry Chemical Physics **23**, 25629–25636 (2021).

[41]A. Sakko, T. P. Rossi, and R. M. Nieminen, "Dynamical coupling of plasmons and molecular excitations by hybrid quantum/classical calculations: time-domain approach," Journal of Physics: Condensed Matter **26**, 315013 (2014).

[42]R. M. Martin, L. Reining, and D. M. Ceperley, *Interacting Electrons: Theory and Computational Approaches* (Cambridge University Press, Cambridge, 2016).

[43]E. Coccia, F. Troiani, and S. Corni, "Probing quantum coherence in ultrafast molecular processes: An *ab initio* approach to open quantum systems," J. Chem. Phys. **148**, 204112 (2018).

[44]M. Marsili and S. Corni, "Electronic Dynamics of a Molecular System Coupled to a Plasmonic

Nanoparticle Combining the Polarizable Continuum Model and Many-Body Perturbation Theory," J. Phys. Chem. C **126**, 8768 (2022).

[45]G. Dall'Osto, M. Marsili, M. Vanzan, D. Toffoli, M. Stener, S. Corni, and E. Coccia, " Peeking into the Femtosecond Hot-Carrier Dynamics Reveals Unexpected Mechanisms in Plasmonic Photocatalysis," J. Am. Chem. Soc. **146**, 2208 (2024).

[46]X. Zhang, X. Li, D. Zhang, N. Su, W. Yang, and H. Everitt, "Product selectivity in plasmonic photocatalysis for carbon dioxide hydrogenation," Nat. Commun. **8**, 14542 (2017).

[47]X. Li, H. O. Everitt, and J. Liu, "Confirming nonthermal plasmonic effects enhance CO_2 methanation on Rh/TiO_2 catalysts," Nano Research **12**, 1906–1911 (2019).

[48]J. C. Tremblay, P. Krause, T. Klamroth, and P. Saalfrank, "Time-dependent response of dissipative electron systems," Phys. Rev. A **81**, 063420 (2010).

[49]G. Füchsel, T. Klamroth, J. C. Tremblay, and P. Saalfrank, "Stochastic approach to laser-induced ultrafast dynamics: the desorption of H_2/D_2 from Ru(0001)," Phys. Chem. Chem. Phys. **12**, 14082 (2010).

[50]G. Floß, T. Klamroth, and P. Saalfrank, "Laser-controlled switching of molecular arrays in an dissipative environment," Phys. Rev. B **83**, 104301 (2011).

[51]G. Füchsel, T. Klamroth, S. Monturet, and P. Saalfrank, "Dissipative dynamics within the electronic friction approach: the femtosecond laser desorption of H_2/D_2 from Ru(0001)," Phys. Chem. Chem. Phys. **13**, 8659 (2011).

[52]M. Schlosshauer, "Decoherence, the measurement problem, and interpretations of quantum mechanics," Rev. Mod. Phys. **76**, 1267–1305 (2005).

[53]A. J. Daley, "Quantum trajectories and open many-body quantum systems," Adv. Phys. **63**, 77 (2014).

[54]P. Saalfrank, "Open-system quantum dynamics for laser-induced DIET and DIMET," Surf. Sci. **390**, 1–10 (1997).

[55]M. Nest and P. Saalfrank, "Open-system quantum dynamics for gas-surface scattering: Nonlinear dissipation and mapped Fourier grid methods," J. Chem. Phys. **113**, 8753 (2000).

[56]H. M. Jaeger, S. Fischer, and O. V. Prezhdo, "Decoherence-induced surface hopping," J. Chem. Phys. **137**, 22A545 (2012).

[57]A. J. Neukirch, Z. Guo, and O. V. Prezhdo, "Time-domain ab initio study of phonon-induced relaxation of plasmon excitations in a silver quantum dot," J. Phys. Chem. C **116**, 15034–15040 (2012).

[58]A. V. Akimov, R. Long, and O. V. Prezhdo, "Coherence penalty functional: A simple method for adding decoherence in Ehrenfest dynamics," J. Chem. Phys. **140**, 194107 (2014).

[59]R. Long and O. V. Prezhdo, "Quantum Coherence Facilitates Efficient Charge Separation at a MoS_2/$MoSe_2$ van der Waals Junction," Nano Lett. **16**, 1996–2003 (2016).

[60]H.-P. Breuer and F. Petruccione, *The Theory of Open Quantum Systems* (Oxford University Press, Oxford, 2006).

[61]H. Carmichael, *Statistical Methods in Quantum Optics 1: Master Equations and Fokker–Planck Equations* (Physics and Astronomy Online Library, Springer, Berlin, 1999).

[62]U. Weiss, *Quantum Dissipative Systems* (World Scientific, Singapore, 2012).

[63]I. Semina, V. Semin, F. Petruccione, and A. Barchielli, "Stochastic schrödinger equations for markovian and non-markovian cases," Open Systems & Information Dynamics **21**, 1440008 (2014).

[64]G. Lindblad, "On the generators of quantum dynamical semigroups," Commun. Math. Phys. **48**, 119–130 (1976).

[65]Y.-S. Wang, P. Nijjar, X. Zhou, D. I. Bondar, and O. V. Prezhdo, "Combining Lindblad master equation and surface hopping to evolve distributions of quantum particles," J. Phys. Chem. B **124**, 4326–4337 (2020).

[66]A. G. Redfield, "The Theory of Relaxation Processes," Adv. Magn. Res. **1**, 1–32 (1965).

[67]D. Egorova, M. F. Gelin, M. Thoss, H. Wang, and W. Domcke, "," J. Chem. Phys. **129**, 214303 (2008).

[68]L. Chen, M. F. Gelin, V. Y. Chernyak, W. Domcke, and Y. Zhao, "Dissipative dynamics at conical intersections: simulations with the hierarchy equations of motion method," Faraday Discuss. **194**, 61–80 (2016).

[69]T. Klamroth, P. Saalfrank, and U. Höfer, "Open-system density-matrix approach to image-potential dynamics of electrons at Cu(100): Energy-and time-resolved two-photon photoemission spectra," Phys. Rev. B **64**, 035420 (2001).

[70]M. Nest and P. Saalfrank, "Open-system density matrix description of femtosecond laser desorption of electronically and vibrationally relaxing adsorbates: Single-and two-pulse scenarios," J. Chem. Phys. **116**, 7189 (2002).

[71]K. Zenichowski, T. Klamroth, and P. Saalfrank, "Open-system density matrix description of an STM-driven atomic switch: H on Si(100)," Appl. Phys. A **93**, 319 (2008).

[72]R. Biele and R. D'Agosta, "A stochastic approach to open quantum systems," J. Phys.: Con-

dens. Matter **24**, 273201 (2012).

[73]H. Haken and P. Reineker, "The coupled coherent and incoherent motion of excitons and its influence on the line shape of optical absorption," Z. Phys. A **249**, 253 (1972).

[74]H. Haken and G. Strobl, "An exactly solvable model for coherent and incoherent exciton motion," Z. Phys. A **262**, 135 (1973).

[75]P. Saalfrank, "Stochastic wave packet vs. direct density matrix solution of Liouville-von Neumann equations for photodesorption problems," Chem. Phys. **211**, 265 (1996).

[76]R. Dum, P. Zoller, and H. Ritsch, "Monte Carlo simulation of the atomic master equation for spontaneous emission," Phys. Rev. A **45**, 4879 (1992).

[77]M. B. Plenio and P. L. Night, "The quantum-jump approach to dissipative dynamics in quantum optics," Rev. Mod. Phys. **70**, 101–144 (1998).

[78]D. Hofmann-Mees, H. Appel, M. D. Ventra, and S. Kümmel, "Determining Excitation-Energy Transfer Times and Mechanisms from Stochastic Time-Dependent Density Functional Theory," J. Phys. Chem. B **117**, 14408 (2013).

[79]N. Gisin and I. C. Percival, "The quantum state diffusion picture of physical processes," J. Phys. A: Math. Gen. **26**, 2245 (1993).

[80]D. E. Makarov and H. Metiu, "Quantum dynamics with dissipation: A treatment of dephasing in the stochastic Schrödinger equation," J. Chem. Phys. **11**, 10126 (1999).

[81]J. Dalibard, Y. Castin, and K. Mølmer, "Wave-function Approach to Dissipative Processes in Quantum Optics," Phys. Rev. Lett. **68**, 580 (1992).

[82]K. Mølmer, Y. Castin, and J. Dalibard, "Wave-function Approach to Dissipative Processes in Quantum Optics," J. Opt. Soc. Am. B **10**, 524 (1993).

[83]J. C. Tremblay, T. Klamroth, and P. Saalfrank, "Time-dependent configuration-interaction calculations of laser-driven dynamics in presence of dissipation," J. Chem. Phys. **129**, 084302 (2008).

[84]J. C. Tremblay, S. Klinkusch, T. Klamroth, and P. Saalfrank, "Dissipative many-electron dynamics of ionizing systems," J. Chem. Phys. **134**, 044311 (2011).

[85]R. D'Agosta and M. Di Ventra, "Stochastic time-dependent current-density-functional theory," Phys. Rev. B **78**, 165105 (2008).

[86]H. Appel and M. Di Ventra, "Stochastic quantum molecular dynamics for finite and extended systems," Chem. Phys. **391**, 27 (2011).

[87]D. G. Tempel and A. Aspuru-Guzik, "Relaxation and Dephasing in Open Quantum Systems

Time-dependent Density Functional Theory: Properties of Exact Functionals from an Exactly-solvable Model System," Chem. Phys. **391**, 130 (2011).

[88]X. Blase, I. Duchemin, and D. Jacquemin, "The bethe–salpeter equation in chemistry: relations with td-dft, applications and challenges," Chem. Soc. Rev. **47**, 1022–1043 (2018).

[89]C. Sissa, F. Delchiaro, F. Di Maiolo, F. Terenziani, and A. Painelli, "Vibrational coherences in charge-transfer dyes: A non-adiabatic picture," J. Chem. Phys. **141**, 164317 (2014).

[90]F. Di Maiolo and A. Painelli, "Intermolecular energy transfer in real time," J. Chem. Theory Comput. **14**, 5339–5349 (2018).

[91]R. Long and O. V. Prezhdo, "Instantaneous Generation of Charge-Separated State on TiO_2 Surface Sensitized with Plasmonic Nanoparticles," J. Am. Chem. Soc. **136**, 4343–4354 (2014).

[92]P. Grobas Illobre, M. Marsili, S. Corni, M. Stener, D. Toffoli, and E. Coccia, "Time-Resolved Excited-State Analysis of Molecular Electron Dynamics by TDDFT and Bethe–Salpeter Equation Formalisms," J. Chem. Theory Comput. **17**, 6314–6329 (2021).

[93]H. Xiong, S. Lin, J. Goetze, P. Pletcher, H. Guo, L. Kovarik, K. Artyushkova, B. M. Weckhuysen, and A. K. Datye, "Thermally stable and regenerable platinum–tin clusters for propane dehydrogenation prepared by atom trapping on ceria," Angew. Chem. Int. Ed. **129**, 9114–9119 (2017).

[94]E. Coccia, G. Dall'Osto, J. Fregoni, G. Gil, M. Marsili, S. Pipolo, M. Romanelli, M. Rosa, and S. Corni, "WaveT-TDPlas," `https://github.com/stefano-corni/WaveT_TDPlas` (2024), [Online; accessed 12-January-2024].

[95]R. Hildner, D. Brinks, and N. F. V. Hulst, "Femtosecond coherence and quantum control of single molecules at room temperature," Nat. Phys. **7**, 172–177 (2010).

[96]D. Brinks, R. Hildner, E. M. H. P. van Dijk, F. D. Stefani, J. B. Nieder, J. Hernando, and N. F. van Hulst, "Ultrafast dynamics of single molecules," Chem. Soc. Rev. **43**, 2476 (2014).

[97]G. W. Robinson and R. P. Frosch, "Electronic Excitation Transfer and Relaxation," J. Chem. Phys. **38**, 1187 (1963).

[98]R. Englman and J. Jortner, "The energy gap law for radiationless transitions in large molecules," Mol. Phys. **18**, 145 (1970).

[99]R. Englman and J. Jortner, "The energy gap law for non-radiative decay in large molecules," J. Lumin. **1-2**, 134 (1970).

[100]J. V. Caspar, B. P. Sullivan, E. M. Kober, and T. J. Meyer, "Application of the energy gap law to the decay of charge transfer excited states, solvent effects," Chem. Phys. Lett. **91**, 91 (1982).

[101]J. S. Wilson, N. Chawdhury, M. R. A. Al-Mandhary, M. Younus, M. S. Khan, P. R. Raithby, A. Köhler, and R. H. Friend, "The Energy Gap Law for Triplet States in Pt-Containing Conjugated Polymers and Monomers," J. Am. Chem. Soc. **123**, 9412–9417 (2001).

[102]C. Doffek, J. Wahsner, E. Kreidt, and M. Seitz, "Breakdown of the Energy Gap Law in Molecular Lanthanoid Luminescence: The Smallest Energy Gap Is Not Universally Relevant for Nonradiative Deactivation," Inorg. Chem. **53**, 3263 (2014).

[103]J. Shi, M. A. Izquierdo, S. Oh, S. Y. Park, B. Milian-Medina, D. Roca-Sanjuan, and J. Gierschner, "Inverted energy gap law for the nonradiative decay in fluorescent floppy molecules: larger fluorescence quantum yields for smaller energy gaps," Org. Chem. Front. **6**, 1948 (2019).

[104]S. J. Jang, "A simple generalization of the energy gap law for nonradiative processes," J. Chem. Phys. **155**, 164106 (2021).

[105]Y. R. Poh, S. Pannir-Sivajothi, and J. Yuen-Zhou, "Understanding the Energy Gap Law under Vibrational Strong Coupling," J. Phys. Chem. C **127**, 5491–5501 (2023).

[106]B. Mennucci and S. Corni, "Multiscale modelling of photoinduced processes in composite systems," Nat. Rev. Chem. **3**, 315 (2019).

[107]S. Corni and J. Tomasi, "Enhanced response properties of a chromophore physisorbed on a metal particle," J. Chem. Phys. **114**, 3739–3751 (2001).

[108]J. Tomasi, B. Mennucci, and R. Cammi, "Quantum mechanical continuum solvation models," Chemical reviews **105**, 2999–3094 (2005).

[109]T. Avanesian and P. Christopher, "Adsorbate specificity in hot electron driven photochemistry on catalytic metal surfaces," J. Phys. Chem. C **118**, 28017–28031 (2014).

[110]M. Vanzan, M. Marsili, and S. Corni, "Study of the rate-determining step of rh catalyzed co2 reduction: Insight on the hydrogen assisted molecular dissociation," Catalysts **11**, 538 (2021).

[111]E. Palik and G. Gosh, *Handbook of Optical Constants of Solids* (Academic Press, San Diego, USA, 1998).

[112]P. Giannozzi, S. Baroni, N. Bonini, M. Calandra, R. Car, C. Cavazzoni, D. Ceresoli, G. L. Chiarotti, M. Cococcioni, I. Dabo, A. D. Corso, G. Fratesi, S. D. Gironcoli, R. Gebauer, U. Gerstmann, C. Gougoussis, A. Kokalj, L. Martin-Samos, N. Marzari, F. Mauri, R. Mazzarello, S. Paolini, A. Pasquarello, L. Paulatto, C. Sbraccia, S. Scandolo, A. P. Seitsonen, A. Smogunov, P. Umari, and R. M. Wentzcovitch, "QUANTUM ESPRESSO: a modular and open-source software project for quantum simulations of materials," J. Phys. Condens. Matter **21**, 395502 (2009).

[113]P. Giannozzi, O. Andreussi, T. Brumme, O. Bunau, M. Buongiorno, M. Marsil, L. Paulatto, and D. Rocca, "Advanced capabilities for materials modelling with Quantum ESPRESSO," J. Condens. Matter Phys. **29**, 465901 (2017).

[114]D. R. Hamann, "Optimized norm-conserving Vanderbilt pseudopotentials," Phys. Rev. B **88**, 085117 (2013).

[115]L. Bengtsson, "Dipole correction for surface supercell calculations," Phys. Rev. B **59**, 12301–12304 (1999).

[116]J. D. Head and M. C. Zerner, "A Broyden—Fletcher—Goldfarb—Shanno optimization procedure for molecular geometries," Chem. Phys. Lett. **122**, 264–270 (1985).

[117]R. Rüger, M. Franchini, T. Trnka, A. Yakovlev, E. van Lenthe, P. Philipsen, T. van Vuren, B. Klumpers, and T. Soini, "Ams 2022.1, scm, theoretical chemistry," (2022).